The effect of interface adhesion on buckling and cracking of hard thin films

Flores-Johnson, E. A.; Shen, L.; Annabattula, R. K.; Onck, P. R.; Shen, Y. G.; Chen, Z.

Published in:
Applied Physics Letters

DOI:
10.1063/1.4900443

Publication date:
2014

The effect of interface adhesion on buckling and cracking of hard thin films

E. A. Flores-Johnson,[1,a)] L. Shen,[1] R. K. Annabattula,[2] P. R. Onck,[3] Y. G. Shen,[4] and Z. Chen[5,6]

[1]*School of Civil Engineering, The University of Sydney, Sydney, NSW 2006, Australia*
[2]*Department of Mechanical Engineering, Indian Institute of Technology Madras, Chennai 600036, India*
[3]*Zernike Institute for Advanced Materials, University of Groningen, 9747 AG Groningen, The Netherlands*
[4]*Department of Mechanical and Biomedical Engineering, City University of Hong Kong, Kowloon, Hong Kong, China*
[5]*Department of Engineering Mechanics, Dalian University of Technology, Dalian 116024, People's Republic of China*
[6]*Department of Civil and Environmental Engineering, University of Missouri, Columbia, Missouri 65211, USA*

(Received 28 August 2014; accepted 13 October 2014; published online 24 October 2014)

The physics behind the strain-released buckling patterns including telephone cords and straight-sided wrinkles with and without cracks, as experimentally observed in sputter-deposited Ti-Si-N thin films on Si substrates, is investigated with model-based simulations by varying the mechanical properties of the interface. Our calculations reveal that the location of the cracks depends on the normal stiffness, the interfacial toughness, and the normal strength of the cohesive interface. These properties determine the geometrical shape of the buckles such as width, wavelength, and deflection, and hence the local bending-induced tensile stresses. Buckling patterns with cracks at the apexes occur for low-stiffness interfaces as well as for high-stiffness interfaces with high toughness. On the other hand, cracks at the bottom of the buckles are more likely to occur for interfaces with high stiffness and low toughness. By using an elastic material model with a fracture criterion for brittle behavior, we demonstrate that the crack will follow the path where the bending-induced principal stress exceeds the flexural strength of the film. © *2014 AIP Publishing LLC*.
[http://dx.doi.org/10.1063/1.4900443]

Thin films have been increasingly used in high-tech industrial applications including microelectronics and thermal barriers.[1,2] Thin films in a Ti–Si–N ternary system, prepared by direct current (DC) reactive magnetron sputtering, exhibit thermal stability and excellent mechanical properties such as high hardness.[3] Adding small amounts of Si into TiN films produces a significant enhancement of hardness when compared with binary nitride TiN films.[4] In these types of films, a maximal hardness (30–50 GPa) can be achieved at Si contents of 6%–12%.[5]

It is well-known that compressive residual stresses generated during the growth of sputter-deposited thin films[6–11] may lead to film decohesion by buckling and delamination, which is detrimental to the integrity and performance of the films.[11] Depending on several factors such as residual stress, film thickness, and interface toughness, delamination can localize and propagate across the film as a buckle of various shapes such as straight-sided wrinkles, telephone cords buckles, or circular blisters.[12,13]

A large body of work exists, including finite-element method (FEM) simulations, in which the formation of different buckling patterns in hard films deposited on rigid substrates is studied, by utilizing a delaminated strip with constant width.[10,12–15] This approach is valid when the interface strength is infinite at the delamination front.[14,16] It has been shown that by taking into account interface adhesion using a cohesive zone model, the kinematics of a propagating telephone cord buckle can be simulated.[17] It has also been demonstrated that the height and width of the buckles are related to the properties of the cohesive zone in both FEM simulations[18,19] and atomistic simulations.[16,20]

Scanning electron microscopy (SEM) images of a $Ti_{0.39}Si_{0.04}N_{0.57}$ thin film grown on a silicon substrate using DC reactive magnetron sputtering[4] showed that various buckling patterns were generated including circular blisters, straight-sided wrinkles, and telephone cords with widths or diameters in the range of 15–25 μm. Moreover, most of the buckling patterns exhibited cracks at their apexes and/or at the bottom of the buckle (Fig. 1). It has been suggested that variations in the interface toughness[4,21] may influence the location of the cracks, but the physics behind the underlying mechanisms leading to the observed buckling and cracking patterns is still not clear.

Inspired by this, we perform model-based simulations to understand how the interface properties such as the normal stiffness, interfacial toughness, and normal strength play a substantial role in controlling buckling shapes and cracking locations.

Figure 2 shows the FE model of a typical thin film bonded to a rigid substrate with a rectangular area of width $W = 60\ \mu$m (along the x axis) and length $L = 120\ \mu$m (along the y axis). There is an initial delaminated zone over a width of $W/3$ and length of 120 μm, which is bounded by two adherent zones of width $W/3$ and length of 120 μm. The substrate is treated as an infinitely rigid body as experimental observations show no damage or deformation on the substrate surface.[4] The film has a thickness of $t = 0.55\ \mu$m and is elastic with the following material properties: Density $\rho = 4900\ \text{kg/m}^3$, Young's modulus $E = 325$ GPa, and Poisson's ratio $\nu = 0.25$.[22]

a)emmanuel.flores-johnson@sydney.edu.au

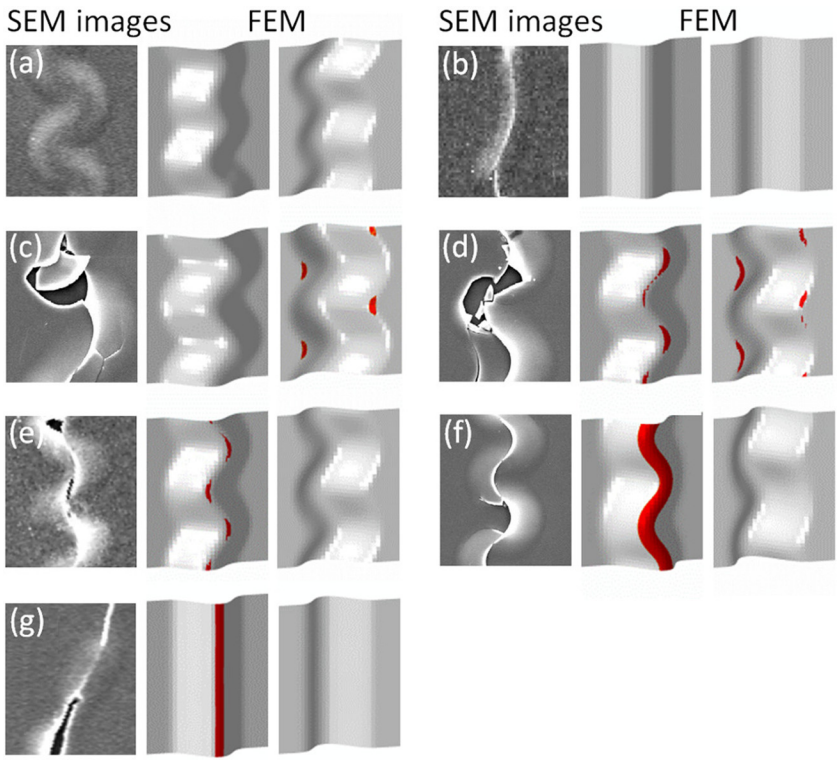

FIG. 1. SEM images of buckling patterns with or without cracks observed in $Ti_{0.39}Si_{0.04}N_{0.57}$ thin film grown on a silicon substrate[4] (left column). Buckling patterns obtained with FEM (right column). Without cracks: (a) Telephone cord and (b) straight-sided wrinkle. With cracks: (c) Telephone cord with discontinuous cracks at the bottom, (d) telephone cord with discontinuous cracks at the apex and at the bottom, (e) telephone cord with discontinuous cracks at the top, (f) telephone cord with continuous crack at the apex, and (g) straight-sided buckle with crack at the apex.

The numerical simulations were carried out using the FE software Abaqus[23] with an explicit solver. For the film, shell elements were employed. For the adherent zones, a cohesive interface obeying a bilinear traction-separation law was used.[23] Damage in the cohesive zone is assumed to initiate when a quadratic interaction function involving the normal and shear tractions T_n and T_t reaches a value of one: $(T_n/T_n^0)^2 + (T_t/T_t^0)^2 = 1$. Here, T_n^0 and T_t^0 are the interface strengths under pure normal and shear loading, respectively. To investigate the effect of the interface on the film buckling, different values of interfacial toughness in mode I, G_I^C, in the range of 4–8 J/m^2 were used.[24,25] For each value of G_I^C, values for G_{II}^C were obtained by considering that $G_{II}^C = \Gamma(\pi/2)$ in the following mixed mode toughness function $\Gamma(\psi) = \{G_I^C\{1 + \tan^2[(1-\lambda)\psi]\}$,[26] where ψ is the mode mixity angle and λ is a parameter that captures the influence of the mode II contribution in the criterion. A value of $\lambda = 0.14$ was used in the simulations based on the range of reported values (0.05–0.25).[17,27] We assumed that $0.02\sigma_0 < T_t^0 < 0.07\sigma_0$,[17] $T_t^0 = 10T_n^0$,[17] and $K_I = 2K_{II}$,[28] with K_I and K_{II} being the normal and shear stiffness of the interface, respectively, and σ_0 being the experimentally reported residual stress.[4]

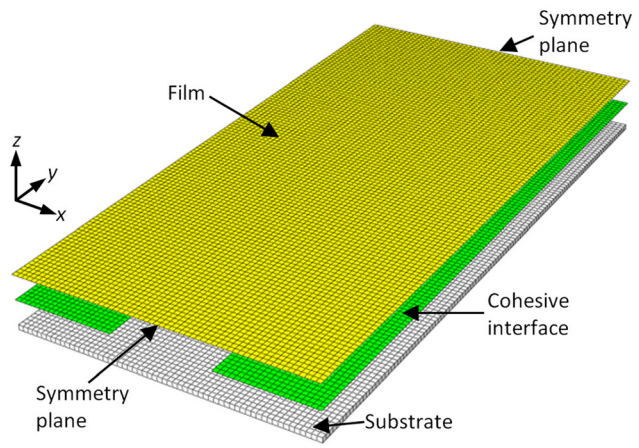

FIG. 2. A typical finite-element 3D mesh for a thin film of width W along the x axis and length L along the y axis with an initial delaminated zone from the substrate over an area of $(W/3) \times L$.

To trigger the buckling, the film is perturbed in the out-of-plane direction with a small imperfection. The loading is governed by an equi-biaxial compressive stress $\sigma_{xx} = \sigma_{yy} = \sigma_0 = -E\epsilon_0/(1-\nu)$,[29] which is achieved by applying an eigenstrain of $\epsilon_0 = 0.01$, calculated from σ_0.[4]

In Fig. 1, we show that the different buckling patterns and crack locations as observed experimentally could be reproduced with the numerical simulations by varying the properties of the cohesive interface. As a criterion to predict in which part of the film a crack is more likely to occur, we highlighted in red color the regions where $\sigma_p/\sigma_0 > 1.15$, with σ_p denoting the maximum in-plane tensile principal stress. Figure 3 describes four maps of the buckling patterns obtained for different normalized stiffnesses $K = \ln(K_I t/\sigma_0)$. In each map, two dimensionless parameters are presented: the normalized normal strength $T = 100(T_n^0/\sigma_0)$ (vertical axis) and the normalized interfacial toughness in mode I $G_I = 1000[G_I^C(1-\lambda)]/(\sigma_0 t)$. The green buckles (left side) are the top view of the film, while the yellow buckles (right side) are the bottom view. Both substrate and cohesive layer are not shown. The red-colored zones mean that in those regions $\sigma_p/\sigma_0 > 1.15$.

The background color coding in the maps indicates crack location in the buckle: at the top (blue), the bottom (pink), top and bottom (green), and no-crack (white). The dashed lines are boundaries for illustrative purposes only. It can be seen that for low stiffness ($K = 1.45$), the film always buckles in a telephone cord shape and is likely to crack at

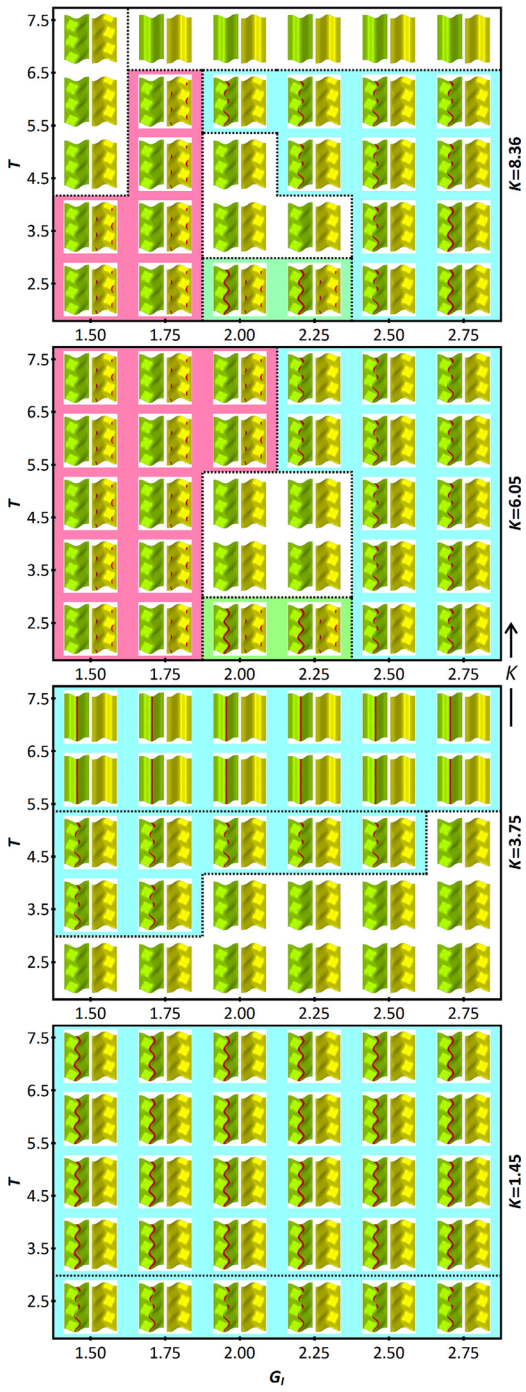

FIG. 3. Maps of buckling patterns for various stiffness values of K plotted against the normalized normal strength and the normalized interfacial toughness. The green buckles are the top view of the film, while the yellow buckles are the bottom view. The red color indicates the regions where $\sigma_p/\sigma_0 > 1.15$. The background color coding indicates crack location in the buckle: At the top (blue), at the bottom (pink), top and bottom (green), and no-crack (white).

the apex of the buckle regardless of interfacial toughness. Failure with a discontinuous crack is predicted at $T < 3$. For $K = 3.75$, the simulations predict that the film will buckle as a straight-sided wrinkle at $T > 5$ and is likely to crack at the top. At $T < 5$, two distinctive regions are observed, namely, telephone cord buckles, which are likely to crack at the top with a discontinuous crack, and telephone cords that will not fail unless larger eigenstrain is applied. The buckling and cracking processes as shown in this map appear to be independent of the interfacial toughness.

For a higher stiffness ($K = 6.05$), two distinctive behaviors are observed, which are highly dependent on the interfacial toughness. For $G_I > 2.1$, the film will buckle as a telephone cord and is likely to crack at the apex with a discontinuous crack. For $G_I < 1.9$, the film buckles as a telephone cord and is likely to fail at the bottom following a localized cracking pattern. This is in agreement with the experiments, in which localized buckling spalling was observed (Figs. 1(c) and 1(d)). A transition zone is observed where the film can fail at the top or the bottom or does not fail. The effect of T is not significant in this map. For the higher stiffness ($K = 8.36$), three distinctive zones are observed. For $G_I > 2.1$ and $T < 6.5$, the film buckles as telephone cord and is likely to fail at the apexes. For $G_I < 2.1$ and $T < 6.5$, the film is likely to fail at the bottom. At $T > 6.5$, a zone where the film will not fail and can buckle either as a telephone cord or as a straight-sided wrinkle is observed. A transition zone is also observed.

Although some transition zones and zones where the film will not fail are observed, we can conclude from the maps that for low stiffness the film tends to fail at the top; while for high stiffness and high interfacial toughness, the film also tends to fail at the top. However, for high stiffness and low interfacial toughness, the film tends to fail at the bottom. This can be explained by the fact that bending induced tension in the film is highly dependent on the geometric shape of the telephone cord buckle. This shape in turn depends on how the compressive strain energy is reduced via three related mechanisms, which are dependent on the interface behavior: energy release by buckling in the z direction (height of the buckle), buckling in the y direction (wavelength of the telephone cord), and buckling in the x direction (delamination).

Figure 4 shows contour plots of the out-of-plane displacement U_z (in μm) for four different cases, where ℓ and $2b$ are the wavelength and width of the telephone cord, respectively. The predicted crack zones ($\sigma_p/\sigma_0 > 1.15$) are also shown in white color. For low stiffness ($K = 1.45$), the film is likely to crack at the top because most of the compressive strain energy is released by buckling in the z-direction (higher U_z). This is independent of the interfacial toughness because for these parameters the cohesive layer behaves elastically without damage. For high stiffness ($K = 6.05$) and low interfacial toughness, the film is likely to fail at the bottom because the larger delamination zone (larger $2b$) and lower ℓ induce high tensile stresses at the bottom due to the larger curvature of the buckle in these zones. For high stiffness and high interfacial toughness, the film is likely to fail at the top because even though ℓ is lower than that of the lower stiffness cases, the delamination is also less and higher bending-induced stresses develop at the top of the buckle. These results are consistent with the available experimental data, in which the telephone cord buckles with cracks at the bottom have larger $2b$ than those with only cracks at the top.[4]

If the bending-induced tensile stress at the apexes exceeds the flexural strength of the film, cracks will initiate. We use a simple fracture criterion to model cracking in the film, by defining a critical tensile strength of 5.1 GPa, above

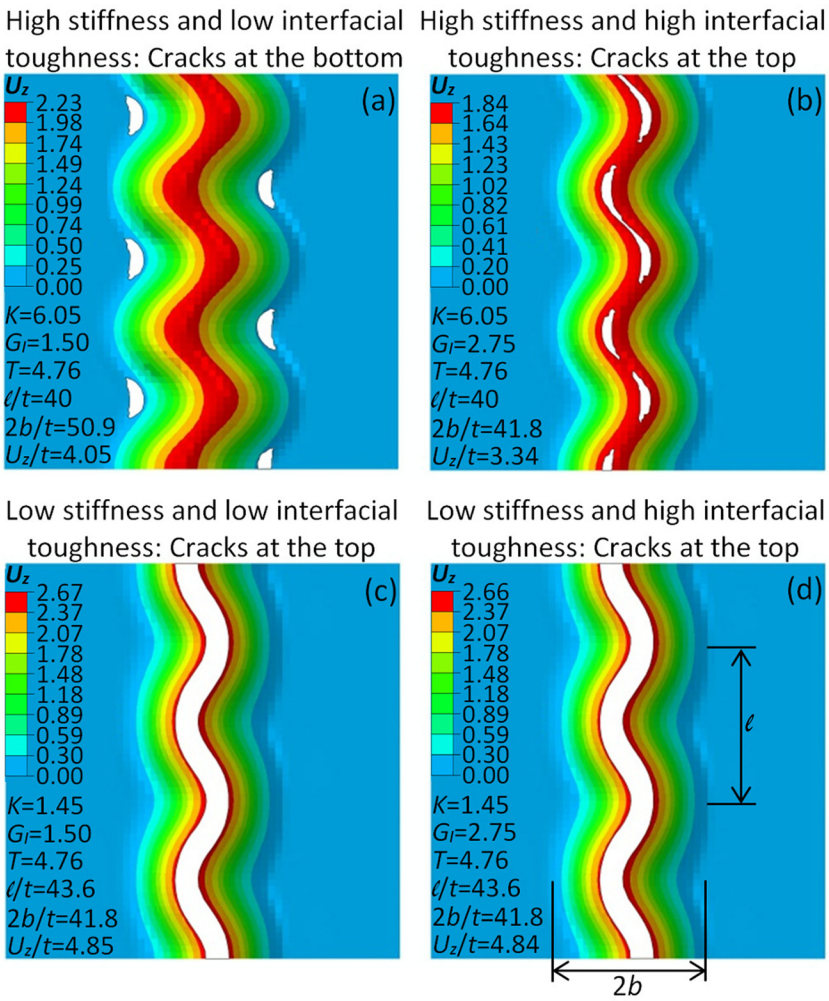

FIG. 4. Contour plots of the out-of-plane displacement U_z (in μm) of telephone cord buckles depicting the width and wavelength for four cases with different interfacial properties: (a) high K and low G_I, (b) high K and high G_I, (c) low K and low G_I, and (d) low K and high G_I. The locations of the cracks are depicted in white color.

which cracking will initiate in the elements (brittle cracking model in Abaqus[23]).

In Fig. 5, we show the normalized principal tensile stress σ_p/σ_0 versus the normalized simulation time τ for elements at the top of the buckle (solid line) and at the bottom of the buckle (dashed line). A contour plot of the out-of-plane deflection of the film when a crack propagates in a telephone cord buckle is depicted showing the location of the elements. The sudden change from negative to positive σ_p/σ_0 ($\tau \approx 0.22$) is related to the buckling onset, while the sudden drop of σ_p/σ_0 at $\tau \approx 0.8$ is related to the cracking onset, resulting in the release of the stored strain energy. These numerical results have already been verified experimentally, showing that the crack propagates at the apex of the buckle.[4] The finding obtained from our model-based simulations further demonstrates that the proposed approach may predict failure in the buckles so that a crack propagating at the apex of a telephone cord buckle can be simulated.

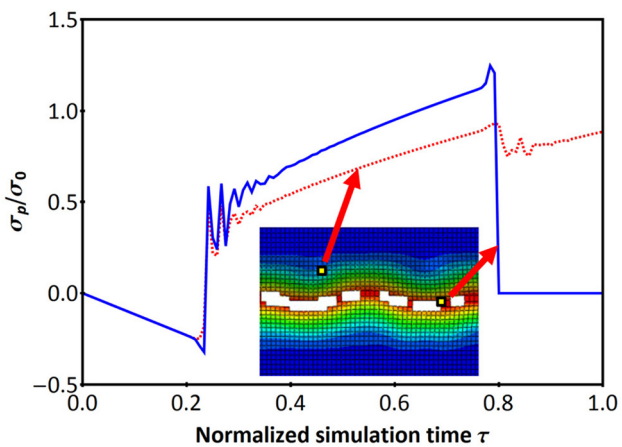

FIG. 5. Normalized principal tensile stress versus the normalized simulation time for two different elements: at the top of the buckle (solid line) and at the bottom of the buckle (dashed line).

In summary, we have demonstrated with our model-based simulations that the various buckling patterns in Ti-Si-N thin film on Si substrate, including telephone cords and straight-sided wrinkles with and without cracks, could be reproduced by varying the mechanical properties of the interface. We showed that the location of cracks depends on the stiffness of the interface, the interfacial toughness, and the normal strength of the cohesive interface. For low-stiffness interface, the film is likely to fail at the top of the buckle because high bending-induced tensile stresses are generated at the apexes due to the large out-of-plane displacement. For high-stiffness interface with low toughness, the film is likely to fail at the bottom because the larger delamination zone and lower buckle wavelength produce large bending-induced tensile stresses in these areas. The use of an elastic material model with a brittle fracture criterion demonstrates that the crack will follow the predicted path where the bending-induced principal stress exceeds the flexural strength of the film.

E.A.F.-J. and L.S. acknowledge the financial support from the Australian Research Council (ARC) Centre of Excellence for Design in Light Metals (CE0561574). This work was also partially supported by the City University of Hong Kong SRG Grant (Project No. 7002755) and the National Natural Science Foundation of China under Grant No. 11232003.

[1]L. B. Freund and S. Suresh, *Thin Film Materials: Stress, Defect Formation, and Surface Evolution* (Cambridge University Press, New York, 2003).
[2]S. Zhang, D. Sun, Y. Fu, and H. Du, Surf. Coat. Technol. **167**, 113 (2003).
[3]L. Rebouta, C. J. Tavares, R. Aimo, Z. Wang, K. Pischow, E. Alves, T. C. Rojas, and J. A. Odriozola, Surf. Coat. Technol. **133–134**, 234 (2000).
[4]Z.-J. Liu, N. Jiang, Y. G. Shen, and X. Li, Thin Solid Films **516**, 7609 (2008).
[5]Y. G. Shen, Z.-J. Liu, N. Jiang, H. S. Zhang, K. H. Chan, and Z. K. Xu, J. Mater. Res. **19**, 523 (2004).
[6]J. W. Hutchinson, M. D. Thouless, and E. G. Liniger, Acta Metall. Mater. **40**, 295 (1992).
[7]L. Shen and Z. Chen, Modell. Simul. Mater. Sci. Eng. **12**, S347 (2004).
[8]M. W. Moon, J. W. Chung, K. R. Lee, K. H. Oh, R. Wang, and A. G. Evans, Acta Mater. **50**, 1219 (2002).
[9]M. W. Moon, H. M. Jensen, J. W. Hutchinson, K. H. Oh, and A. G. Evans, J. Mech. Phys. Solids **50**, 2355 (2002).
[10]G. Parry, A. Cimetière, C. Coupeau, J. Colin, and J. Grilhé, Phys. Rev. E **74**, 066601 (2006).
[11]F. Vaz, L. Rebouta, P. Goudeau, J. P. Rivière, E. Schäffer, G. Kleer, and M. Bodmann, Thin Solid Films **402**, 195 (2002).
[12]M. W. Moon, K. R. Lee, K. H. Oh, and J. W. Hutchinson, Acta Mater. **52**, 3151 (2004).
[13]R. K. Annabattula and P. R. Onck, J. Appl. Phys. **109**, 033517 (2011).
[14]B. Audoly, Phys. Rev. Lett. **83**, 4124 (1999).
[15]G. Parry, J. Colin, C. Coupeau, F. Foucher, A. Cimetière, and J. Grilhé, Appl. Phys. Lett. **86**, 081905 (2005).
[16]K. Pan, Y. Ni, and L. He, Phys. Rev. E **88**, 062405 (2013).
[17]J.-Y. Faou, G. Parry, S. Grachev, and E. Barthel, Phys. Rev. Lett. **108**, 116102 (2012).
[18]R. K. Annabattula, W. T. S. Huck, and P. R. Onck, J. Mech. Phys. Solids **58**, 447 (2010).
[19]F. Gruttmann and V. D. Pham, Comput. Mech. **41**, 361 (2008).
[20]A. Ruffini, J. Durinck, J. Colin, C. Coupeau, and J. Grilhé, Scr. Mater. **67**, 157 (2012).
[21]J. S. Wang and A. G. Evans, Acta Mater. **47**, 699 (1999).
[22]F. Vaz, S. Carvalho, L. Rebouta, M. Z. Silva, A. Paúl, and D. Schneider, Thin Solid Films **408**, 160 (2002).
[23]Simulia, Abaqus Analysis User's Manual (version 6.11).
[24]S. Benayoun, J. J. Hantzpergue, and A. Bouteville, Thin Solid Films **389**, 187 (2001).
[25]R. H. Dauskardt, M. Lane, Q. Ma, and N. Krishna, Eng. Fract. Mech. **61**, 141 (1998).
[26]J. W. Hutchinson and Z. Suo, Adv. Appl. Mech. **29**, 63 (1991).
[27]A. Lee, C. S. Litteken, R. H. Dauskardt, and W. D. Nix, Acta Mater. **53**, 609 (2005).
[28]E. A. Flores-Johnson, L. Shen, I. Guiamatsia, and G. D. Nguyen, Compos. Sci. Technol. **96**, 13 (2014).
[29]S. Edmondson, K. Frieda, J. E. Comrie, P. R. Onck, and W. T. S. Huck, Adv. Mater. **18**, 724 (2006).